Solution Structure and Dynamics of Oxytetracycline Polyketide Synthase Acyl Carrier Protein from *Streptomyces rimosus*[†,‡]

Stuart C. Findlow,[§] Claire Winsor,[§] Thomas J. Simpson,[||] John Crosby,[||] and Matthew P. Crump*[,§,||]

School of Biological Sciences, University of Southampton, Bassett Crescent East, Southampton, SO16 7PX, United Kingdom, School of Chemistry, University of Bristol, Cantock's Close, Bristol BS8 1TS, United Kingdom

Received February 7, 2003; Revised Manuscript Received May 15, 2003

ABSTRACT: Type II polyketide synthases (PKSs) utilize a dedicated and essential acyl carrier protein (ACP) in the biosynthesis of a specific polyketide product. As part of our ongoing studies into the mechanisms and control of polyketide biosynthesis, we report the second structure of a polyketide synthase ACP. In this work, multidimensional, heteronuclear NMR was employed to investigate the structure and dynamics of the ACP involved in the biosynthesis of the commonly prescribed polyketide antibiotic, oxytetracycline (otc). An ensemble of 28 structures of the 95 amino acid otc ACP (9916Da) was computed by simulated annealing with the inclusion of 1132 experimental restraints. Atomic RMSDs about the mean structure for all 28 models is 0.66 Å for backbone atoms, 1.15 Å for all heavy atoms (both values calculated for the folded part of the protein (residues 3−80)), and 0.41 Å for backbone atoms within secondary structure. Otc ACP adopts the typical right-handed, four-helix fold of currently known ACPs but with the addition of a 13-residue flexible C-terminus. A comparison of the global folds of all structurally characterized ACPs is described, illustrating that PKS ACPs show clear differences as well as similarities to FAS ACPs. ^{15}N relaxation experiments for the protein backbone also reveal that the long loop between helices I and II is flexible and helix II, a proposed site of protein−protein interactions, shows conformational exchange. The helices of the ACP form a rigid scaffold for the protein, but these are interspersed with an unusual proportion of flexible linker regions.

Discovered in 1945, oxytetracycline (otc) and chlortetracycline (*1*−*3*) (Figure 1) were the first of a series of related polyketide (*4*) compounds displaying potent antimicrobial activity. As inhibitors of protein synthesis they are excellent therapeutic agents and the first antibiotics to be described as "broad-spectrum". Through overuse, the efficacy of oxytetracycline has declined due to the acquisition by sensitive strains of resistance determinants from the otc producer, *Streptomyces rimosus*. The strategy of modifying existing drugs has proved highly effective at overcoming such inherited resistance mechanisms in pathogenic species. The chemical alteration of tetracyclines to give the glycylcyclines has yielded a class of compounds with potent antimicrobial activity against tetracycline-resistant strains that express both ribosomal protection and efflux determinants (*5*−*7*). It has been proposed that an understanding of the biosynthetic mechanisms involved in the synthesis of polyketides such as oxytetracycline could lead to intelligent, programmable manipulation of the drug assembly process to yield novel polyketide products (*8*).

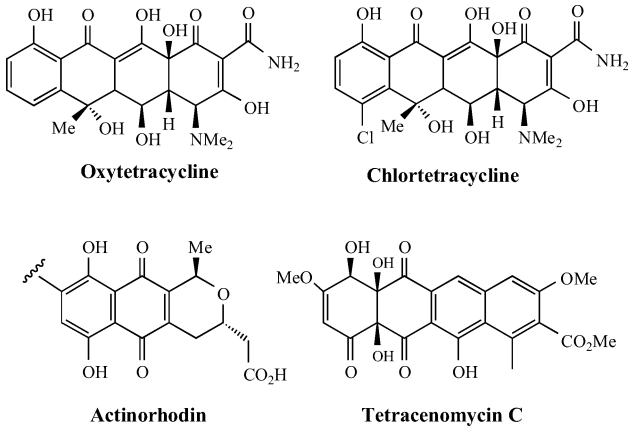

FIGURE 1: Aromatic polyketides from type II PKSs.

Polyketide biosynthesis follows a similar mechanistic pathway to fatty acid synthesis whereby successive decarboxylative condensations of malonate moieties onto a starter unit (typically acetate) yield a hydrocarbon chain (fatty acid) or a highly functionalized carbon chain (polyketide) (*9*). Acyl carrier proteins play an essential role in the formation of both fatty acid and polyketide products. In the type II synthases found in bacteria (*10*) and plants (*11*), ACPs are small acidic proteins of about 80 residues which are

[†] This work was supported by an equipment grant from the Wellcome Trust to the University of Southampton (055640 to M.P.C. and S.C.F.).

[‡] The chemical shift assignments have been deposited at the BioMagResBank with accession number 5664, and the ensemble of 28 structures has been deposited at the Brookhaven PDB with the access code 1NQ4.

* Corresponding author. Present address: University of Bristol. Phone: 0117 3317163. Fax: 0117 9298611. E-mail: matt.crump@bristol.ac.uk.

[§] University of Southampton.

[||] University of Bristol.

[1] Abbreviations: ACP, acyl carrier protein; CLF, chain length factor; FAS, fatty acid synthase; KS, ketosynthase; otc, oxytetracycline; NOE, nuclear Overhauser enhancement; NRPS, non-ribosomal peptide synthase; PCP, peptidyl carrier protein; PKS, polyketide synthase; RMSD, root-mean-square deviation.

10.1021/bi0342259 CCC: $25.00
Published on Web 06/25/2003

posttranslationally modified from the inactive apo protein to the active holo ACP by the transfer of a 4′-phosphopantetheine group from coenzyme A to a conserved serine on the ACP by holo ACP synthase (*12*). NMR studies have provided solution structures for the type II ACPs from the *Streptomyces coelicolor* actinorhodin (act) polyketide synthase (*13*), *Bacillus subtilis* FAS (*14*), *Escherichia coli* FAS (*15*), *Mycobacterium tuberculosis* FAS (*16*), and the expressed domain of the type I rat FAS (*17*). In addition the three-dimensional structures of the discrete D-alanyl PCP from *Lactobacillus rhamnosus* (*18*) and the modular PCP from *Bacillus brevis* (*19*) have been solved. These studies have suggested that ACPs and PCPs have a common topology consisting of a distorted four α-helical bundle. The arrangement of the conserved serine at the N-terminus of helix II is well conserved, but the structures can vary in terms of helical alignment, length, and surface charge. Recent crystal structures have also indicated a site of protein−protein interaction between *B. subtilis* ACP and ACPS (*20*). This again lies along helix II, and this site has been proposed to be the point of interaction of all of the discrete FAS proteins (*21*). Given the similarities of the acyl carrier protein three-dimensional structures it was initially suggested that ACPs from different organisms or different pathways (*22*) could be interchanged in vivo or in vitro to give a functioning synthase. More recently however, work on FAS enzymes from a number of organisms (*23*−*25*) as well as the in vitro minimal PKS (ACP−KS−CLF) assay (*26*) have highlighted examples where ACP substitution resulted in an inactive complex. Therefore despite similar global folds, ACPs are not simply interchangeable between FAS and PKS systems (which produce nonfunctional synthases) (*22*), between PKSs (which can yield functional synthases but the distribution of polyketide products is altered) (for a review see, ref *27*) and between NRPSs and FASs (a PCP was modified by a FAS ACPS but only by replacing helix II of the PCP from *B. brevis* with that of *B. subtilis* FAS ACP) (*28*). In these cases subtle differences in structure must be evident, and detailed comparisons of carrier proteins from a range of organisms and biosynthetic pathways are required to illuminate these differences.

The oxytetracycline PKS however displays a number of characteristics that may place additional demands on the protein−protein interactions mediated by the otc ACP. First, disruption of the aromatase/cyclase (ARO/CYC) gene (*otcD1*) in the *S. rimosus* PKS gene cluster led to loss of chain length control and yielded a mixture of truncated polyketide chains (*29*). This suggested significant interaction of the ARO/CYC with the minimal PKS and a possible role in chain length determination. This could therefore involve the ACP and the bound polyketide, requiring the ACP to mediate multiple interactions. Second, the otc PKS may preferentially select malonamyl-CoA as a starter unit rather than acetate requiring specific protein−protein interactions to override the normal starter selection (*29*). Genetic analyses of those systems which use an alternate starter (*30*) reveal the presence of additional genes, including a putative CoA ligase (*otcY2*−*3*) in *S. rimosus* that may be involved in the biosynthesis of malonamyl-CoA (*31*).

The architecture of the association between the enzymes and the acyl carrier protein is part of our ongoing studies to elucidate the priming and early stage mechanisms of polyketide biosynthesis. We report here the solution structure and dynamical behavior of the oxytetracycline polyketide synthase ACP from *S. rimosus*. We have investigated this PKS ACP by multinuclear, multidimensional NMR that extends earlier studies of the act PKS ACP from *S. coelicolor* and complements our ongoing NMR and X-ray crystallographic studies of type I ACPs (*17*) and other FAS and PKS (gris, gra, and fren) type II ACPs. The otc and act ACPs show similar three-dimensional folds and have a common angular variation in helix I when compared to FAS ACPs. This is contrary to claims that this variation may be due to the quality of the original act structure (*14*). This is also the first full relaxation study of an ACP that shows that the PKS ACP is essentially well folded with a structured scaffold but the protein contains an unusual number of mobile residues. Further within the structured core, helix II, a proposed site of protein−protein interaction shows slow conformational exchange. Dynamics studies have also revealed that the otc ACP structure has a long flexible C-terminal loop not observed in other PKS ACPs. In this paper we also show that the loop between helices I and II is flexible and contrast this to examples of FAS ACPs.

MATERIALS AND METHODS

NMR Experimental Data. The apo- form of unlabeled and ^{15}N-labeled otc ACP was prepared and characterized by ESMS as previously described (*32*). Typically the lyophilised protein was dissolved to a final concentration of 2mM in 90%H_2O/10%D_2O, 2mM DTT, 0.01mM NaN_3, and 30mM sodium deuteroacetate at pH 5.3. Standard NMR experiments were acquired as described previously (*13*), including pulsed-field gradient-assisted 3D ^{15}N NOESY-HSQC and 3D ^{15}N TOCSY-HSQC experiments (*33*) which were carried out on either a 600 MHz Varian *INOVA* Spectrometer (University of Southampton) or a Varian Unity 600 MHz spectrometer (University of Edinburgh). These datasets were recorded at 25 °C with WATERGATE water suppression (*34*). Mixing times of 150 and 65 ms were employed for the 3D NOESY-HSQC and 3D TOCSY-HSQC, respectively. The data were processed using nmrPipe (*35*) and viewed with nmrDraw and PIPP (*36*). Assignment of ^{1}H and ^{15}N chemical shifts was achieved using a standard sequential assignment strategy (*37*), and 60 HN−Hα dihedral angles were measured from an HNHA spectrum. Eighteen $^1\chi$ angles were calculated using relative NOE intensities from a 50ms mixing time 3D NOESY-HSQC and coupling constants from a 2D COSY spectrum.

Slowly Exchanging Amide Protons. For the characterization of slowly exchanging amide protons, a sample of otc ACP was prepared as above using 100% ^2H_2O as solvent and a final pD_{corr} of 4.78. A series of ^{1}H-^{15}N HSQC spectra were immediately recorded at 500 MHz and 20 °C at averaged times of 1, 4.5, 16, 37, and 70 h after the protein was dissolved in D_2O. Amide peaks observable after 16 and 37 h were described as exhibiting slow and very slow exchange.

Conformational Restraints and Structure Calculations. XPLOR (3.81) was used to anneal and calculate a final family of 28 structures using 1054 distance constraints (including 147 long-range NOEs) and 78 dihedral angle restraints. PIPP was used to measure NOE peak volumes

from 3D NOESY-HSQC experiments with a mixing time of 150ms with cross-peak intensities classified as strong, medium, weak, and very weak and assigned to respective interproton distance categories of 1.8−2.3, 1.8−3.0, 1.8−3.5, and 1.8−4.5 Å. Seventy-six hydrogen bond restraints coordinating 38 hydrogen bonds principally within helices were employed on the basis of slow amide exchange data ($CO_i-NH_{i+4} = 1.3-2.3$ Å, $CO_i-N_{i+4} = 2.3-3.3$ Å). Further restraints for hydrogen bond pairs Ala33(CO)−Leu37(NH), Phe34(CO)−Gly38(NH), Thr68(CO)−Phe34(NH), and Leu4-(NH)−Asn78(γO) were added after modeling indicated initially unidentified hydrogen bond receptors for the remaining slow exchange amide protons.

^{15}N Backbone Dynamics. ^{15}N T_1 and T_2 and NOE relaxation data for otc ACP were recorded at 25 °C using a Varian *INOVA* 600 MHz NMR spectrometer. {^{1}H}-^{15}N NOEs were measured by recording HSQC spectra with and without proton saturation. The spectra were recorded without NOE with inter scan delays of 5 s and with NOE using 3 s of proton saturation and 2 s of delay to give the same total delay of 5 s between scans. All spectra were processed with the program NMRpipe. T_1, T_2, and NOE spectra were automatically picked using the program CAPP (*35*), and T_1 and T_2 values were obtained by nonlinear least-squares fits of the amide cross-peak intensities to a two parameter exponential decay using software provided by Lewis E. Kay. Uncertainties in the T_1 and T_2 values were estimated from the nonlinear least-squares fits. Uncertainties in the NOE values were estimated from the baseplane noise in two-dimensional ^{1}H-^{15}N-HSQC spectra recorded with and without proton saturation according to Farrow et al., (*38*).

The theoretical basis for T_1, T_2 and NOE relaxation of ^{15}N is well established and related to a spectral density function at ^{1}H and ^{15}N frequency combinations (ω) (*39*). The data are related to motional parameters using the "model-free" assumption for the correlation function (*40*, *41*) where the spectral density function is

$$J(\omega) = 2/5(S^2\tau_m/(1 + (\omega\tau_m)^2) + (1 - S^2)\tau/(1 + (\omega\tau)^2)) \quad (1)$$

where τ_m is the overall correlation time (isotropic tumbling is assumed), S^2 is the order parameter, $\tau^{-1} = \tau_m{}^{-1} + \tau_e{}^{-1}$ and τ_e is the effective correlation time describing fast internal motions. These are referred to as $S^2 - \tau_m$ or $S^2 - \tau_m - \tau_e$ models, depending on whether a fast motion is required for the fit or not. Two further models were considered that incorporated conformational exchange as an R_{ex} (s^{-1}) term in the T_2 equations (*39*) and are referred to as $S^2 - \tau_m - R_{ex}$ or $S^2 - \tau_m - \tau_e - R_{ex}$ depending on where a τ_e term is included in the latter model. In addition internal motions were accounted for with a two timescale model (*42*, *43*).

RESULTS AND DISCUSSION

We have investigated the structure of oxytetracycline ACP using multidimensional, multinuclear NMR. In common with other ACPs we have studied, crosspeaks in the HSQC spectra were well resolved and remained of high quality over time. The structure was determined using 978 NOEs and 76 hydrogen bond restraints based on slow amide exchange. Sixty ϕ and 18 $^1\chi$ dihedral angle restraints were also incorporated on the basis of NMR measurements for residues where conformational averaging was not observed; i.e., where coupling constants were not averaged (7 Hz), chemical shift degeneracy did not occur, and NOE intensity at a mixing time of 50ms was indicative of restricted mobility.

In the final calculation, 60 structures were generated using XPLOR. Of these, 28 models were selected on the basis of their combined lack of restraint violations, small deviations from ideal bonds and angles, and energetic favorability. A structure with the lowest RMSD to the average of the final 28 models was selected as the most representative model or "average" structure and used for detailed study and comparisons. All experimental restraints were well satisfied with no NOE violations exceeding 0.3 Å (Table 1). Over 95% of ϕ and $^1\chi$ dihedral angles for the 28 models, excluding the 13 residue unstructured C-terminus, fell in the most favorable or favorable regions of the Ramachandran plot. Residues regularly falling in the generously allowed regions included Ser41 and Gln58. Figure 2 shows a best fit superposition of the 28 structures with otc ACP. The structure resolution is high, with the backbone RMSD over residues 3−80 being 0.66 Å. There is a clear correlation between the well-defined structure over helices I−IV and residues 30−40, and the number of restraints per residue over this region. Few restraints are observed for the residues 19−29 and the C-terminal loop. Excluding these regions, the backbone RMSD drops to 0.44 Å.

The structure consists of a folded amino terminal unit (residues 3−80) and a highly flexible, structurally undefined carboxyl terminus comprising approximately 13 residues (residues 83−95) (Figures 2 and 3). The folded part of the protein, like all previously studied ACPs, forms a right turn distorted helical bundle. Secondary structure is dominated by three main helices (helices I (res 6−17), II (res 41−55) and IV (res 71−80)) and a fourth, short less well-defined helix III (res 62−67). The three main helices are of approximately equal length and the four helices adopt a down-up-down-up conformation. Helix I lies at an angle of ~60° to helices II and IV, which in turn are roughly parallel. A slightly distorted type 1 β-turn (res 60−63) precedes helix III, which also lies at ~60° to helices II and IV but at 90° to helix I (see Figure 3).

Helix I (Leu6 to Ala17) is preceded by a short stretch of well-defined extended structure that packs closely to helix IV (Arg71 to Thr82) and Tyr55 of helix II. A long 23 residue loop (loop 1) (Ala18 to Tyr40) connects helices I and II. The first half of loop 1 (Ala18 to Val29) is ill-defined and flexible, indicated by a lack of short-range NOEs, and the RMSD for residues 18−29 is subsequently large (1.37 ± 0.43 and 2.55 ± 0.79 Å for backbone and heavy atoms, respectively). However, the second half of loop 1 (Glu30 to Asp40) is well structured supported by many short- and long-range NOEs and H-bonds identified from exchange rate data and structure calculations. Figures 2 and 3 illustrate the spatial freedoms of this region that appear to allow the loop to flex vertically within approximately 5 Å while maintaining the overall loop shape.

Loop 2 (res 56−70) forms contacts to the helix core in the form of Gln58−Leu81 and Leu59−Ser80 and ends with a slightly distorted type I β-turn (Gly60−Ala63) prior to helix III. Helix III is short and essentially only a single turn (Ala63−Ala67). The turn between helix III and IV adopts no regular turn conformation but is rigidly held in position

Table 1: Structural Statistics and Atomic RMS Differences for 28 Calculated Otc ACP Structures

		⟨28 otc ACP⟩	otc ACP
RMS deviations from experimental			
all NOE & H-bond (1054)		0.0227 ± 0.0037	0.023
distance restraints (Å)[a]	intraresidue (257)	0.0274 ± 0.0041	0.030
	sequential ($\|i-j\|=1$) (340)	0.0193 ± 0.0021	0.019
	short ($1<\|i-j\|<5$) (74)	0.0221 ± 0.0031	0.021
	long ($\|i-j\|\geq 5$) (94)	0.0288 ± 0.0060	0.025
	short (R^{-6} averaged) (20)	0.0102 ± 0.0033	0.010
	long (R^{-6} averaged) (53)	0.0324 ± 0.0049	0.037
	H-bonds (76)	0.0184 ± 0.0024	0.017
angle restraints (deg)	dihedral angles (78)	0.1780 ± 0.0990	0.138
energies (kcal mol^{-1})[b]	E_{NOE}	26.54 ± 3.4369	27.02
	E_{DIHE}	0.152 ± 0.0646	0.096
	E_{REPEL}	32.86 ± 4.2837	30.06
deviations from idealized geometry[c]	bonds (Å)	0.0026 ± 0.0002	0.0026
	angles (deg.)	0.5213 ± 0.0126	0.5213
	improper (deg.)	0.3180 ± 0.0129	0.3134
RMSD (Å)[d]	backbone atoms (3−80)	0.93 ± 0.22	0.39
	backbone atoms (3−18, 3−80)	0.62 ± 0.15	0.37
	heavy atoms (3−80)	1.62 ± 0.28	0.72
	heavy atoms (3−18, 30−80)	1.25 ± 0.18	0.72
(ϕ/ψ) in Ramachandran plot (%)[e]			
residues 3−80	core region	80.6	81.4
	additionally allowed regions	16.1	15.7
	generously allowed regions	3.1	2.9
	forbidden regions	0.2	0
residues 3−18, 30−80	core region	88.3	88.5
	additionally allowed regions	9.4	8.2
	generously allowed regions	2.3	3.3
	forbidden regions	0	0

[a] The RMS deviation of the experimental restraints is calculated with respect to the upper and lower limits of the input restraints. [b] The values for E_{NOE} and E_{DIHE} are calculated from a square well potential with a force constant of 50 kcal mol^{-1} Å^2 and 200 kcal mol^{-1} rad^{-2}. E_{REPEL} is calculated with a force constant of 4 kcal mol^{-1} Å^{-4}, and the final van der Waals radii were set to 0.80 times the value used in the CHARMM force field. [c] The values for bonds, angles, and impropers show the deviation from ideal values based on perfect stereochemistry. [d] Root-mean-square deviations to the average structure. [e] As determined by the program PROCHECK (*44*).

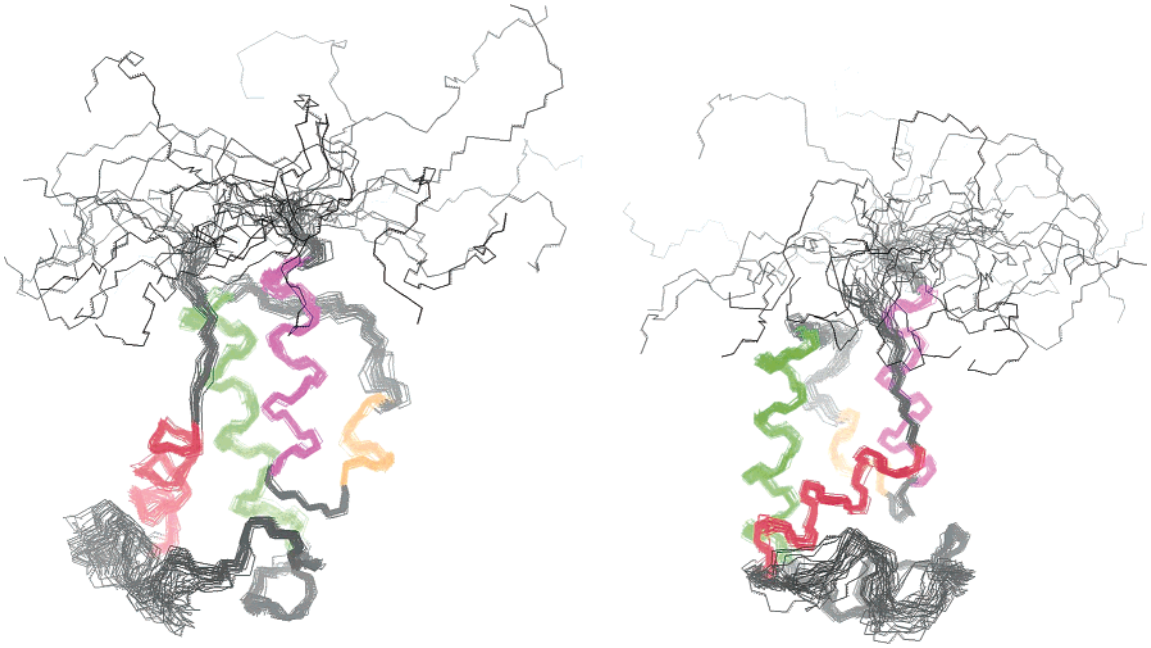

FIGURE 2: Superimposed backbone (N, C$^\alpha$, C) trace of the final 28 models of otc ACP viewed from two angles. Helices are colored red (helix I), green (II), orange (III), and magenta (IV). All residues 1−95 are shown, and the best fit was taken over residues 3−18 and 30−80.

by a plethora of NOEs connecting the turn to many residues in loop 1. The final 13 amino acids following helix IV adopt no specific geometry as predicted from the lack of NOE restraints.

Arg71 is highly conserved in PKS ACPs and exhibits some interesting behavior in the NMR datasets. The ϵ-proton shows a large downfield chemical shift at 9.15 ppm compared to more typical values for such a resonance at 7.2−7.4 ppm. This downfield shift is indicative of the ϵ-proton being hydrogen bonded. Two NOEs can be distinguished from Arg71 ϵ-^{1}H to the α and β protons of Asp31. This suggests Asp31 (which is also highly conserved in polyketide ACPs)

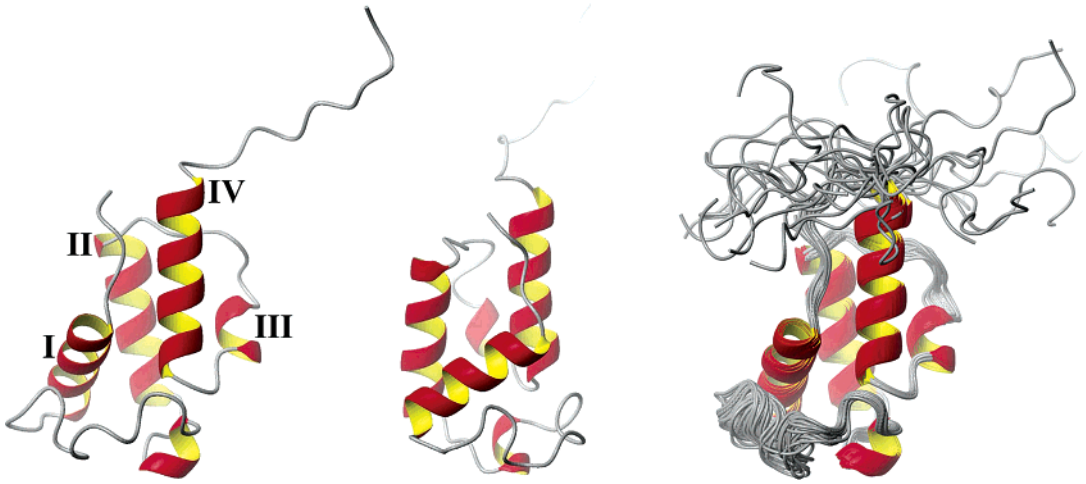

FIGURE 3: The solution structure of otc ACP (left and center) viewed from two angles and the superimposed set of 28 models (right). All graphics were generated using MOLMOL (*45*).

to be the hydrogen bond receiver; however, models suggest it is Glu30 that is more structurally aligned. Whichever salt bridge is formed, it seems likely that the interaction is strong since the resonances for Arg71 δ protons are inequivalent. Chemical shift degeneracy of arginine δ protons is common and indicative of a freely mobile, often solvent-exposed side chain (*46*). However, the chemical shift difference of Arg71 δ-protons in otc ACP is 0.34 ppm. Similarly four separate resonances are observed for the four side chain protons of Glu30, supporting the possibility that Arg71 and Glu30 are the interacting pair. However, the most interesting observation regarding Arg71 is the presence of peaks corresponding to the protons on one of the terminal amine groups. Such resonances are normally exchange broadened (due to rapid proton on/off rates catalyzed by the delocalized positive charge present on arginine) to such an extent they are not visible (*46*). It appears that just one NH_2 group is exchange stable since both observed proton resonances correlate to a single ^{15}N frequency. The models show Arg71 is not significantly buried but Glu30, Asp31 (conserved), and Glu75 are potential hydrogen bond partners for the guanadinium protons.

^{15}N Dynamics. Relaxation data for T_1, T_2, and NOE relaxation were obtained for 82 out of 95 residues (Figure 4). Residues 40, 47 and 50 gave no fit, and at the C-terminus of the protein, 85, 89, 90, 91, 92, and 94 also failed to fit any model. Therefore, motional parameters for 74 residues in total were reliably extracted. Analysis of the data for otc shows that the data fall into four groups. First, helices I and IV both show a predominance of data fit by the simpler $S^2 - \tau_m$ or $S^2 - \tau_m - \tau_e$ models with high S^2 values. This reflects that structurally both helices I and IV are among the most well-defined in otc and the act PKS ACP NMR structures. In the family of otc NMR structures, helices I and IV superimpose with an RMSD of 0.39 $\pm$ 0.09 Å, whereas helices I and II and helices II and IV superimpose with RMSDs of 0.46 $\pm$ 0.14 and 0.46 $\pm$ 0.13 Å, respectively. The second group is comprised of residues at the C-terminal tail of otc ACP. Helix IV terminates at Thr82 and both Thr82 and Gly83 are fit best by the two-time-scale model. Beyond these residues the T_1 and T_2 values rise toward the C-terminus and, where fits could be obtained, the S^2 values are much reduced. The dynamics study reveals that the C-terminus is essentially unstructured from Gly83 to Lys95.

The third group is comprised of the loop regions of otc ACP between residues 20 to 33 and 56 to 62. Loop 1 shows elevated T_1 values and elevated T_2 values with the exception of Leu25. Subsequently the loop shows significantly reduced order parameters and a number of residues fit only the two time-scale model. Leu25 shows a large exchange parameter, having a very short T_2 (71 ms). Structurally this region is devoid of long-range NOEs with the exception of Ser22, Ile23 and Leu25 that show contacts to helix I and Tyr39. However, in this instance the NOE may be slightly misleading, and its averaging behavior (*47*) can bias the closest approach of the two contributing protons. Therefore, the structures may only reflect the loop populating a state that brings these hydrophobes within close proximity to helix I, where in fact it samples a greater conformational space, as reflected by the dynamics data. This is in contrast to the recent study of the *M. tuberculosis* ACP, where ^1H-^{15}N NOE was measured over the entire ACP sequence (*16*). Although a full dynamics study was not performed, the NOE values observed were constant over the loop and of a similarly high value to the remainder of the protein. This is backed up by the structural data where several hydrophobic contacts were observed between the loop and the helical core. The structure calculations therefore revealed that the loop is not flexible and has a defined structure. In the second loop of otc ACP, there is again an increase in T_1 values and a less pronounced increase in T_2 values. Leu59 interestingly shows only a poor fit to the data for T_1. It is unclear at present why this is the case, except that we have observed that this amide proton is extremely sensitive to temperature, pH, and salt concentrations and can change its proton shift by up to 1 ppm (similarly for Ile60 in act acp).

The fourth group of residues are clustered on helix II and are characterized by fits to the S^2-R_{ex} and S^2-τ_e-R_{ex} models (Leu42 0.67s^{-1}; Val48 0.65s^{-1}; Gly49 0.98s^{-1}; Glu52 1.49s^{-1}; Arg53 1.78s^{-1}; Asp54 0.96s^{-1}). These slower exchange motions do not however manifest themselves as an observable flexibility in the NMR structures. The 28 NMR models would suggest that this helix is ordered and is as well-defined as helices I and IV, a result of numerous short and long-range NOEs. The motions of these residues are not isolated and are also observed on adjacent residues in loop

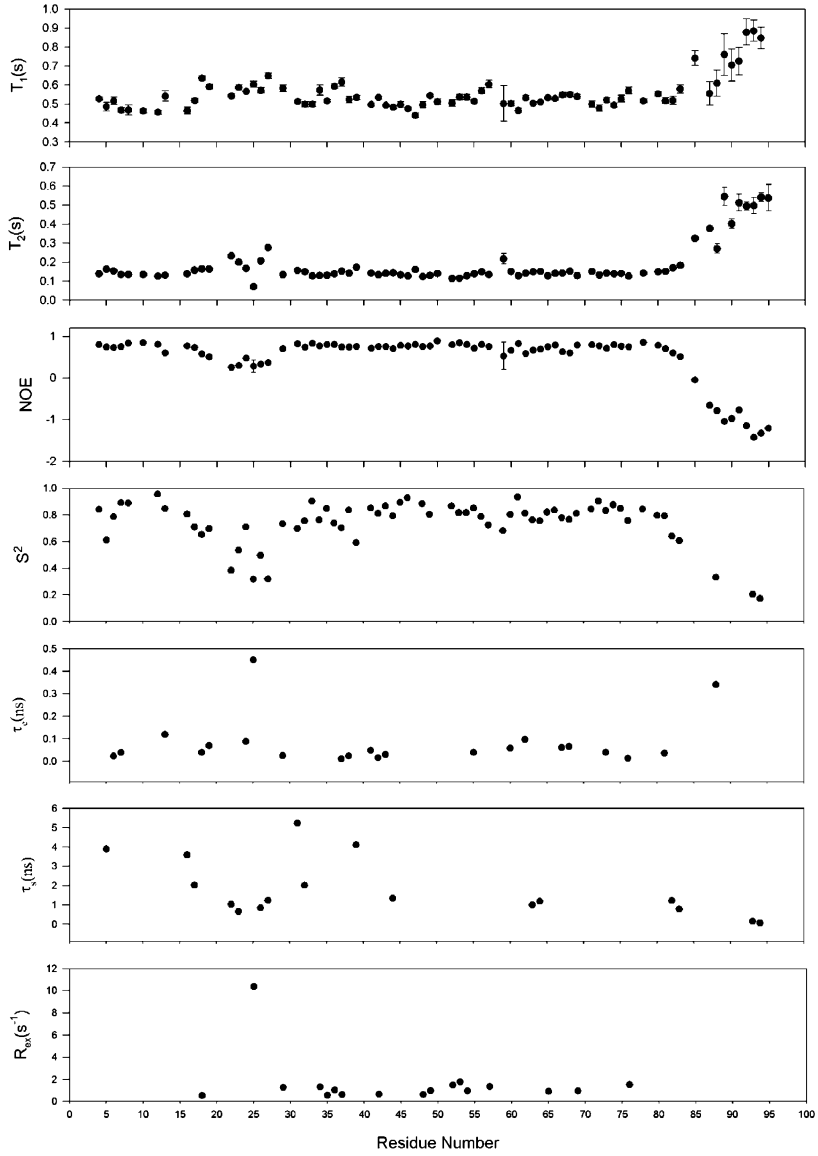

FIGURE 4: Relaxation data for otc ACP at three magnetic fields. Plots of ^{15}N-T_1 (A), ^{15}N-T_2 (B), and NOE (C) at 600 {●} MHz. Graphical representation of dynamics parameters derived from the Lipari & Szabo model free analysis (*40*, *41*). (D) Order parameters (S^2), (E) internal correlation times (τ_e), and (F) two time scale (τ_s) and (G) conformational exchange terms (R_{ex}) parameters are plotted as a series of sequential plots.

2 (Val57 1.36s^{-1}; Leu59 1.69s^{-1}) and helix IV (Met76 1.54s^{-1}). Figure 5 shows a ribbon representation of the motions of the protein where the ribbon thickness is inversely proportional to S^2 and dark blue shading is incremented on the basis of the observed R_{ex} value. In this orientation the interaction of the C-terminus of helix II with the central portion of helix IV and loop 2 is visible.

Comparison of otc ACP with Other ACP Structures. ACP structures are now available for fatty acid moieties from *E. coli* (*15*), *M. tuberculosis* (*16*), and *B. subtilis* (either free (*14*) or in complex with ACP synthase (*20*)), the discrete alanyl carrier protein from *L. casei* (*18*), the polyketide ACP from *S. coelicolor* (*13*) and the type I rat FAS ACP domain (*17*). Table 2 lists a comprehensive set of RMSD values illustrating the relative quality of the otc ACP structure and its similarity to other ACP folds. The quality of the folded segment of otc ACP (residues 3−84) is not as high as that obtained for the ACP from *M. tuberculosis (*ACPM) (section A). However, a similar calculation performed on residues 3−17 and 30−84 (i.e., exclusion of the first half of loop 1 and the C-terminal tail) suggests the quality of both sets of structures to be almost identical. ACPM appears to have a well-structured, rigid loop 1, whereas in otc ACP it is highly flexible. The ^{15}N relaxation properties of this region indicate that the flexibility is not due to missing restraints in otc ACP, and similar results have been reported for *S. coelicolor* (PKS), *B. subtilis* (FAS) and *E. coli* (FAS) ACPs. NMR data collected on ACPM from *M. tuberculosis* and alanyl carrier protein from *L. casei* suggest that region is well defined (*16*, *18*). Therefore, flexibility in the loop is not attributable to either the FAS or PKS ACPs.

Helix I. Table 2, part B, lists RMSDs of the PKS otc ACP overlaid on ACPs from a PKS source (act ACP) and FAS sources (*E. coli*, *B. subtilis* (Bsub), and ACPM) as well as RMSD values obtained from overlaying *E. coli* FAS ACP on the PKS ACPs. Superimposing otc residues 8−80 and equivalents from the other ACPs shows that the PKS ACPs are more similar to each other than any of the FAS ACPs with RMSDs of 2.73 and 3.4−4.0 Å, respectively. Equally the FAS ACPs overlay more accurately on each other than

Table 2: Summary of RMSD Values Derived from Superimposing Structurally Characterized ACPs over Various Regions of Sequence

A								
	full length		res 3−84		res 3−17 30−84		6−17 41−55 71−84	
RMSDs relative to mean /Å[a]	backbone	heavy	backbone	heavy	backbone	heavy	backbone	heavy
otc28 overlay	4.08	4.40	0.66	1.14	0.45	0.89	0.41	0.88
ACPM 20 overlay	3.99	4.34	0.42	0.89	0.44	0.93	0.43	1.05
act 24 overlay	1.72	2.11	1.44	1.89	0.99	1.50	0.82	1.34

B				
pairwise RMSD/Å	otc res 8−80	otc 8−17, 42−80	otc 8−17, 42−55, 71−80	otc 42−80
otc on act	act res 9−81	act 9−18, 43−81	act 9−18, 43−56, 72−81	act 43−81
	2.73	1.72	1.36	1.74
otc on ACPM	acpm res 8−80	acpm 8−17, 42−80	acpm 8−17, 42−55, 71−80	acpm 42−80
	3.40	2.16	2.00	1.78
otc on Bsub	Bsub res 3−75	Bsub 3−12, 37−75	Bsub 3−12, 37−50, 66−75	Bsub 37−75
	4.02	2.97	2.8	2.19
otc on *E. coli* (xtal)	*E. coli* res 3−75	*E. coli* 3−12, 37−75	*E. coli* 3−12, 37−50, 66−75	*E. coli* 37−75
	3.70	2.88	3.13	1.53
E. coli on act	4.01	2.44	2.59	1.72
E. coli on acpm	2.07	2.21	3.70	1.60
E. coli on Bsub	2.11	1.85	1.31	1.90

[a] All values were calculated using the "fit" routine as implemented in MolMol (*45*).

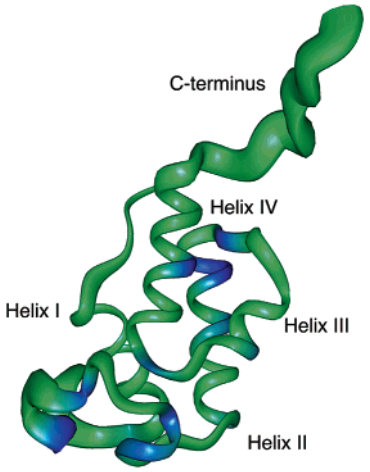

FIGURE 5: Ribbon diagram of otc ACP where the ribbon thickness is proportional to the amplitude of fast internal motions 1-S^2. Residues that exhibit conformational exchange (significant R_{ex} terms) are shaded in blue with the depth of color proportional to the size of the R_{ex} term (600 MHz).

on PKS ACPs. Excluding loop 1 from the calculations narrows the range in which the RMSD values drop, although PKS/PKS and FAS/FAS superimpositions still generate the lowest figures. Overlaying just the three major helices gives lower RMSD values, although in roughly the same ratios (*E. coli*/ACPM being the only exception). Conversely, an overlay of the region from helix II to IV results in very similar RMSDs, be it PKS/PKS, FAS/FAS, or PKS/FAS. Indeed the lowest RMSD is generated when otc PKS ACP is compared to *E. coli* FAS ACP. Thus, it seems the greatest variability in structure appears to be the positioning of helix I relative to the rest of the protein. Figure 6 illustrates the superimpositions of otc ACP on act ACP, *E. coli* ACP, *M. tuberculosis* ACPM, *B. subtilis* ACP and *L. casei* alanyl carrier protein, viewing helix I side on. Helix I in the two PKS ACPs aligns closely but with a 2 Å axial displacement. However, when otc ACP is overlaid with the FAS ACPs, it is clear that there is a rotational displacement of helix I. In the PKS ACPs, the N-terminus of helix I is in contact with the N-terminus of helix IV, as opposed to being positioned midway along helix IV in the FAS ACPs. This rotation is most extreme in alanyl carrier protein, where helix I runs almost antiparallel to helices II and IV and the N-terminus of helix I is in close proximity to the C-terminus of helix IV. This angular displacement results in helix I in the FAS ACPs needing to be slightly longer than that in the PKS ACPs in order to maintain contact with helices II and IV at its C- and N-termini, respectively. These contacts are preserved by an additional turn of helix I in ACPM and half-turns in the other FAS ACPs. Nevertheless, the C-terminal end of helix I is spatially conserved with respect to helix II in all five ACPs shown in Figure 6. Models of *E. coli* FAS ACP binding to *E. coli* KASIII (*21*) suggest helix II to be the recognition helix for FAS enzymes but also indicate that Glu13 from the C-terminus of helix I may play a role. A mutation V17C in the *E. coli* ACP has been shown to reduce FAS activity by 50%, whereas recognition by ACPS was mostly unaffected (12% reduction in holo levels) (*48*). In the otc ACP, the C-terminus of helix I contains the unusual free cysteine (Cys16 and conserved in a number of type II PKS ACPs) (Figure 7), whose role is yet to be determined but which could play a part in polyketide biosynthesis. The large number of proteins with which ACPs are thought to interact means that this helix I angular variation between PKS and FAS ACPs may yet prove significant. In reporting the *B. subtilis* ACP structure (*14*), the authors make extensive claims that the differences between the act ACP structure and the *B. subtilis* structure are attributable to the NMR methods used. Although less precise, the act structure was not inaccurate, and this is borne out by the observation that the higher quality otc structure shows similar differences to the FAS ACPs.

Helix II. In nearly all ACPs, the phosphopantetheine cofactor is covalently bound to a serine residue in a "DSL" sequence motif at the N-terminus of helix II (Ser41 in otc). *B. subtilis* ACP binds ACPS through interactions of the DSL motif and helix II with positively charged residues on ACPS (*20*). The *B. subtilis* ACPS was shown to modify a chimeric ACP constructed from the helix II of *B. subtilis* ACP and

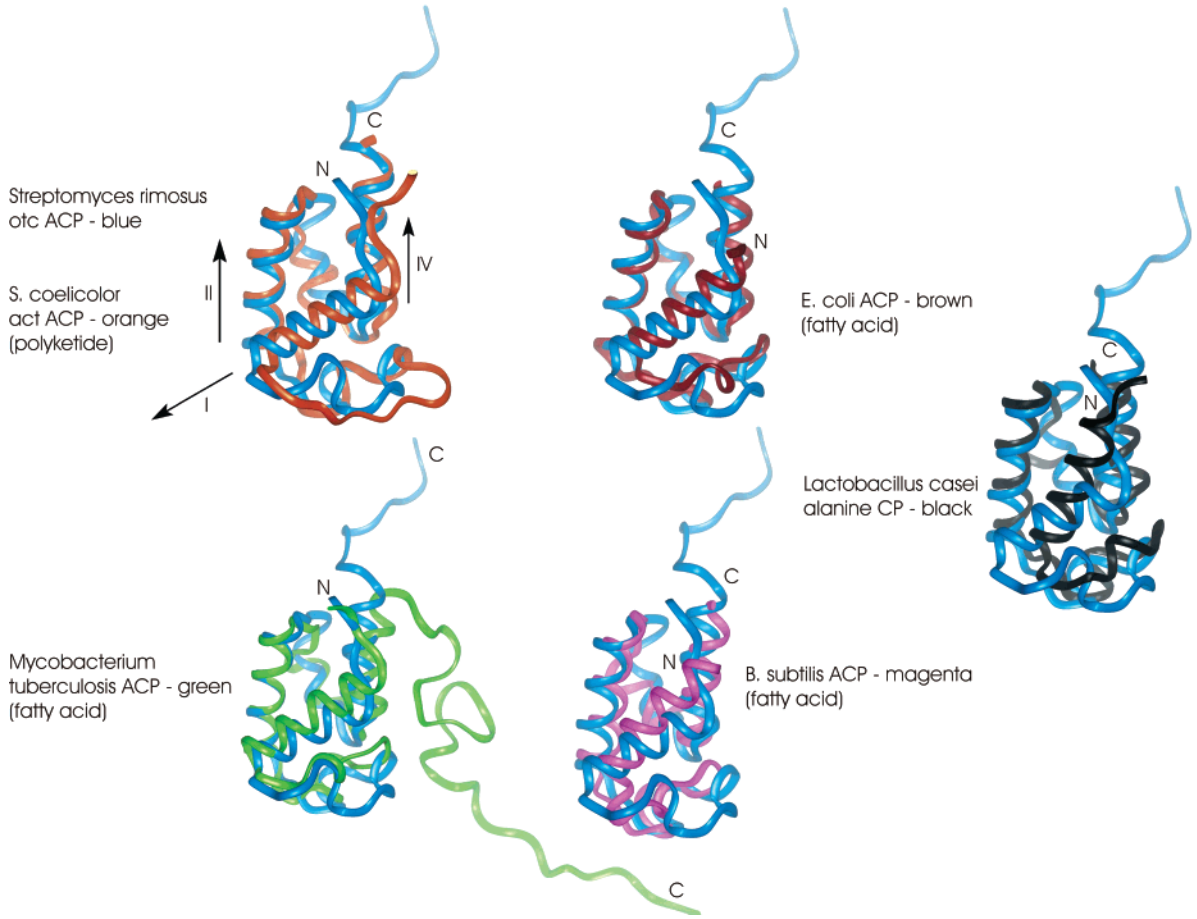

FIGURE 6: Superimpositions of otc ACP (blue) on various known ACP structures. Only helices II, III, and IV and the connecting loops were superimposed to highlight the variable positioning of helix I.

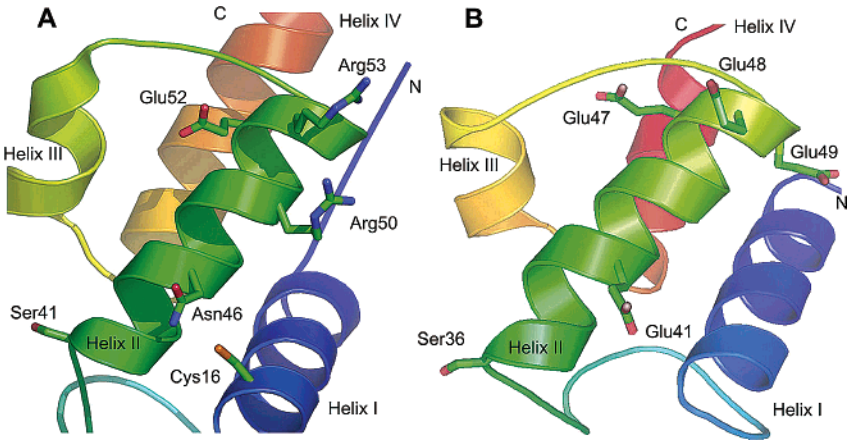

FIGURE 7: Cartoon representation of (A) otc ACP and (B) *E. coli* ACP. Several negatively charged residues are shown for *E. coli* ACP, including Glu41 and Glu47, Glu48 and Glu49, that have been implicated in FAS binding. A different arrangement of positive and negative charge is shown for otc ACP.

the remaining scaffold of a PCP but was inactive with the wild-type PCP (*28*). Modeling studies have been extended to *E. coli* ACP−KASIII complexes and show the highly conserved Glu41 interacting with Arg249 on the surface of KASIII. Mutation of Arg249 led to a loss in activity of KASIII and loss of ACP binding. In addition, Glu41 of the *Vibrio harveyi* ACP has recently been shown to be important for FAS activity but not acyl-ACP synthetase activity (*49*). Otc ACP does not have this conserved Glu, but has an Asn at the equivalent position (Asn46) on helix II (Figure 7). This is unusual for a type II PKS ACP and analysis of 15 other type II PKS ACPs shows this position is always a glutamate with the exception of glycine in the curomycin producer *S. curacoi*. *E. coli* KASIII activity and ACP binding was also sensitive to the mutation of basic residues identified as partners for Glu47, Glu48, and Glu49 in *E. coli* ACP (Figure 7). However, otc shows a mixture of positive charges (Arg50, Arg53), and negative charges (Glu52, Asp54) at the C-terminus of helix II. Therefore, although helix II may be an important recognition site for PKS ACPs, only the presence of the correct positive/negative residues may ensure correct KS/CLF binding. This could be why different PKS

ACPs are not simply interchangeable and this is currently under further study.

The C-Terminus. The unusual random coil carboxyl terminus of otc ACP consists of seven alanines and glycines, one proline, and five polar or charged residues producing a highly flexible and solvent-exposed tail. The carboxyl terminus of ACPM is substantially longer at 35 amino acids. Helix IV ends at approximately the same position as that in otc ACP, but whereas residues 82−95 in otc ACP are random coil, residues 82−96 in ACPM adopt a "molten" state and are described as being relatively ordered (*16*) and show NOE contacts from "molten domain" residues to the main fold of the protein. ACPM residues 97−115 are random-coil in nature. The function(s) of this unusual feature in these ACPs is still unknown. Suggestions have been made (*16*) that, since ACPM is involved in the synthesis of very long chain mycolic acids, it interacts with only long chain intermediates and adopts no regular structure in the non-derivatized holo protein. Carrying this idea across to polyketides would suggest that oxytetracycline is an abnormally long chain antibiotic; however, this is not the case (backbone 19 carbon atoms). Another suggestion (*16*) is that the tail forms an additional protein−protein interaction. Comparison of the aligned sequences of otc ACP and ACPM shows that residues 82−96 contain a high proportion of alanines and contain a proline, a lysine, and an arginine misaligned by just one amino acid. Salt bridges from the Lys/Arg to acidic residues located variably on other pathway enzymes may serve to stabilise complex formation. Such sequence similarities leads one to speculate that protein−protein interaction is perhaps a more logical role for the tail although in ACPM these residues form part of the molten domain and are not as flexible and solvent-exposed as in otc ACP.

Inherent flexibility is a common theme in regions of proteins involved in protein−protein or protein−nucleic acid interactions (*50*). We have compared the relaxation data for otc ACP with a number of other small proteins whose data were available in the Indiana Dynamics Database (IDD) and within our group. The average S^2 is 0.86 ± 0.06 (98%) (Human Cardiac Troponin C), 0.83 ± 0.04, (Human Eotaxin), 0.83 ± 0.06 (95%) (Glutaredoxin-1), 0.85 ± 0.03 (88%) (Ubiquitin), 0.85 ± 0.04 (Chymotrypsin Inhibitor-2), 0.84 ± 0.03 (81%) (Calbindin (free)), 0.88 ± 0.07 (90%) (IL-4), and 0.86 ± 0.04 (84%) (C-terminal Kunitz Domain) using residues with $NOE^{500} > 0.60$ and $NOE^{600} > 0.65$. The figure in brackets is the number of residues whose $NOE^{600} > 0.65$ or $NOE^{500} > 0.60$ expressed as a percentage of the total number of residues measured. For otc ACP, the average S^2 is 0.82 ± 0.05 over residues with NOE > 0.65, only slightly lower than the average figures reported for other small proteins that have been studied by ^{15}N relaxation. However, the number of residues with NOE > 0.65 is only 67% of the total, significantly lower than above where 89% on average are above 0.65. This is partly attributable to a long flexible C-terminal tail in otc ACP, which is either absent or much shorter in the proteins analyzed above. Excluding the C-terminus of otc ACP gives a number of 75%, still appreciably lower than above. Interestingly the dynamics studies described here suggest that although helix II appears well-structured in the NMR models, many of its residues undergo a small amount of conformational exchange. This is not on the same scale as that seen for *E. coli* ACP where extremely fast amide exchange was observed for Ser36, Leu37, Asp38, Thr39, Glu41, Ala45, and Leu46 in helix II ($k_{ex} > 0.70$ min^{-1}) (*51*), while we observed that helix II amides are more highly protected in otc ACP (data not shown). Nevertheless, a small amount of flexibility in helix II may allow for distortion in an ACP−PKS complex. Helix II is heavily implicated as an important protein−protein recognition site, and flexibility may allow the protein to accommodate an interaction with another protein or modulate the binding affinity through the quenching or nonquenching of these motions.

The otc ACP presents a picture where a scaffold (which itself has elements that are flexible) is surrounded by flexible sites, perhaps allowing some distortion of the structure. In the case of the otc ACP (and other polyketide ACPs), multiple protein recognition sites and flexibility may be of particular importance since the protein must interact with numerous enzymes. For priming it must interact with the holo synthase enzyme for conversion to the holo form. During elongation of the polyketide it will interact with the ketosynthase enzyme as well as the chain length factor (from *otcY1),* followed by a reductase (*otcY2*) and the bifunctional ARO/CYC (*otcD1*). There is also the possibility that several of these enzymes will simultaneously interact with the otc ACP. Disruption of the *otcD1* gene product has been shown to produce four shunt products (LH1-LH4) that all contain the correct malonamide starter unit but have truncated and misfolded carbon chain lengths (*29*). It is speculated therefore that ARO/CYC is required along with the ACP−KS−CLF and KR to form a properly integrated complex. Indeed the KR does not perform its reduction in the absence of the ARO/CYC (*29*). The possibility that the ACP aids in the fidelity of the polyketide processing by interacting with these synthase components is a tantalising concept that were are currently pursuing.

ACKNOWLEDGMENT

We thank John Rafferty of the Molecular Biology and Biotechnology Centre at the University of Sheffield for supplying the coordinates of the *E. coli* ACP structure and John Parkinson of the School of Chemistry at the University of Edinburgh for several NMR datasets used in conjunction with this work. We would also like to thank the Wellcome Trust for the spectrometer equipment grant (055640) and support for S.C.F. We also thank Lewis Kay at the University of Toronto for pulse sequences.

REFERENCES

1. Finlay, A. C., Hobby, G. L., P'an, S. Y., Regna, P. P., Routien, J. B., Seeley, D. B., Shull, G. M., Sobin, B. A., Solomons, I. A., Vinson, J. W., and Kane, J. H. (1950) Terramycin, a new antibiotic, *Science 111,* 85.
2. Hochstein, F. A., Stevens, C. R., Conover, L. H., Regna, P. F., Pasternack, R., Gordon, P. N., Pilgrim, F. J., Brunings, K. J., and Woodward, R. B. (1953) The structure of terramycin, *J. Am. Chem. Soc. 75,* 5455−5475.
3. Silver, L., and Bostian, K. (1990) Screening of natural products for antimicrobial agents, *Eur. J. Clin. Microbiol. Infect. Dis. 9,* 455−461.
4. O'Hagan, D. (1991) in *The Polyketide Metabolites* (Mellor, J., Ed.) Ellis Horwood Series in Organic Chemistry, Ellis Horwood Limited, Chichester, U.K.
5. Barden, T. C., Buckwalter, B. L., Testa, R. T., Petersen, P. J., and Lee, V. J. (1994) "Glycylcyclines". 3. 9-Aminodoxycycline-carboxamides, *J. Med. Chem. 37,* 3205−3211.

6. Eliopoulos, G. M., Wennersten, C. B., Cole, G., and Moellering, R. C. (1994) In vitro activities of two glycylcyclines against gram-positive bacteria. *Antimicrob. Agents Chemother. 38*, 534−541.
7. Testa, R. T., Petersen, P. J., Jacobus, N. V., Sum, P. E., Lee, V. J., and Tally, F. P. (1993) In vitro and in vivo antibacterial activities of the glycylcyclines, a new class of semisynthetic tetracyclines, *Antimicrob. Agents Chemother. 37*, 2270−2277.
8. Kramer, P. J., Zawada, R. J. X., McDaniel, R., Hutchinson, C. R., Hopwood, D. A., and Khosla, C. J. (1997) Rational Design and Engineered Biosynthesis of a Novel 18-Carbon Aromatic Polyketide, *J. Am. Chem. Soc. 119*, 635−639.
9. Hopwood, D. A. (1997) Genetic contributions to understanding polyketide synthases, *Chem. Rev. 97*, 2465−2497.
10. Rawlings, M., and Cronan, J. E. (1992) The gene encoding *Escherichia coli* acyl carrier protein lies within a cluster of fatty acid biosynthetic genes, *J. Biol. Chem. 267*, 5751−5754.
11. Baerson, S. R., Vanderheiden, M. G., and Lamppa, G. K. (1994) Identification of domains in an Arabidopsis acyl carrier protein gene promoter required for maximal organ-specific expression, *Plant Mol. Biol. 26*, 1947−1959.
12. Lambalot, R. H., Gehring, A. M., Flugel, R. S., Zuber, P., LaCele, M., Marahiel, M. A., Reid, R., Khosla, C., and Walsh, C. T. (1996) A new enzyme superfamily − the phosphopantetheinyl transferases, *Chem. Biol. 3*, 923−936.
13. Crump, M. P., Crosby, J., Dempsey, C. E., Parkinson, J. A., Murray, M., Hopwood, D. A., and Simpson, T. J. (1997) Solution structure of the actinorhodin polyketide synthase acyl carrier protein from *Streptomyces coelicolor*, *Biochemistry 36*, 6000−6008.
14. Xu, G.-Y., Tam, A., Lin, L., Hixon, J., Fritz, C. C., and Powers, R. (2001) Solution structure of *Bacillus subtilis* acyl carrier protein, *Structure 9*, 277−287.
15. Kim, Y., and Prestegard, J. H. (1990). Refinement of the NMR structures for acyl carrier protein with scalar coupling data, *Proteins 8*, 377−385.
16. Wong, H. C., Liu, G., Zhang, Y.-M., Rock, C. O., and Zheng, J. (2002) The solution structure of acyl carrier protein from *Mycobacterium tuberculosis*, *J. Biol. Chem. 277*, 15874−15880.
17. Reed, M. A. C., Schweizer, M., Szafranska, A. E., Arthur, C., Nicholson, T. P., Cox, R. J., Crosby, J., Crump, M. P., and Simpson, T. J. (2003) The isolated acyl carrier protein domain from the type I rat fatty acid synthase shows considerable structural homology and analogous biochemical properties to type II acyl carrier proteins, *Org. Biol. Chem. 3*, 463−471.
18. Volkman, B. F., Zhang, Q., Debabov, D. V., Rivera, E., Kresheck, G. C., and Neuhaus, F. C. (2001) Biosynthesis of D-Alanyl-Lipoteichoic Acid: The tertiary structure of apo-D-Alanyl carrier protein, *Biochemistry 40*, 7964−7972.
19. Weber, T., Baumgartner, R., Renner, C., Marahiel, M. A., and Holak, T. A. (2000) Solution structure of PCP, a prototype for the peptidyl carrier domains of modular peptide synthetases, *Struct. Folding Des. 8*, 407−418.
20. Parris, K. D., Lin, L., Tam, A., Mathew, R., Hixon, J., Stahl, M., Fritz, C. C., Seehra, J., and Somers, W. S. (2000) Crystal structures of substrate binding to *Bacillus subtilis* holo-(acyl carrier protein) synthase reveal a novel trimeric arrangement of molecules resulting in three active sites, *Structure Folding Des. 8*, 883−895.
21. Zhang, Y. M., Rao, M. S., Heath, R. J., Price, A. C., Olson, A. J., Rock, C. O., and White, S. W. (2001) Identification and analysis of the acyl carrier protein (ACP) docking site on beta-ketoacyl-ACP synthase III, *J. Biol. Chem. 276*, 8231−8238.
22. Khosla, C., Ebertkhosla, S., and Hopwood, D. A. (1992) Targeted gene replacements in a *Streptomyces* polyketide synthase gene cluster − role for the acyl carrier protein, *Mol. Microbiol. 6*, 3237−3249.
23. Crosby, J., Byrom, K. J., Hitchman, T. S., Cox. R. J., Crump, M. P., Findlow, I. S., Bibb, M. J., and Simpson, T. J. (1998) Acylation of Streptomyces type II polyketide synthase acyl carrier proteins, *FEBS Lett. 433*, 132−138.
24. Florova, G., Kazanina, G., and Reynolds, K. A. (2002) Enzymes involved in fatty acid and polyketide biosynthesis in *Streptomyces glaucescens*: role of FabH and FabD and their acyl carrier protein specificity, *Biochemistry 41*, 10462−10471.
25. Ritsema, T., Gehring, A. M., Stuitje, A. R., van der Drift, K. M., Dandal, I., Lambalot, R. H., Walsh, C. T., Thomas-Oates, J. E., Lugtenberg, B. J., and Spaink, H. P (1998) Functional analysis of an interspecies chimera of acyl carrier proteins indicates a specialized domain for protein recognition, *Mol. Gen. Genet. 257*, 641−648.
26. Matharu, A. L., Cox, R. J., Crosby, J., Byrom, K. J., and Simpson, T. J. (1998) MCAT is not required for *in vitro* polyketide synthesis in a minimal actinorhodin polyketide synthase from *Streptomyces coelicolor*, *Chem. Biol. 5*, 699−711.
27. Staunton, J., and Weissman, K. J. (2001) Polyketide biosynthesis: a millennium review, *Nat. Prod. Rep. 18*, 380−416.
28. Mofid, M. R., Finking, R., and Marahiel, M. A. (2002) Recognition of hybrid peptidyl carrier proteins/acyl carrier proteins in nonribosomal peptide synthetase modules by the 4′-phosphopantetheinyl transferases AcpS and Sfp. *J. Biol. Chem. 277*, 17023−17031.
29. Petkovic, H., Thamchaipenet, A., Zhou, L. H., Hranueli, D., Raspor, P., Waterman, P. G., and Hunter, I. S. (1999) Disruption of an aromatase/cyclase from the oxytetracycline gene cluster of *Streptomyces rimosus* results in production of novel polyketides with shorter chain lengths, *J. Biol. Chem. 274*, 32829−32834.
30. Moore, B. S., and Hertweck, C. (2002) Biosynthesis and attachment of novel bacterial synthase starter units, *Nat. Prod. Rep. 19*, 70−99.
31. Hunter, I. S., and Hill, R. A. (1997) in *Biotechnology of Antibiotics*, 2nd ed. (Strohl, W. R., Ed.) pp 659−682, Marcel Decker Inc., New York.
32. Cox, R. J., Hitchman, T. S., Byrom, K. J., Findlow, I. S., Tanner, J. A., Crosby, J., and Simpson, T. J. (1997) Post-translational modification of heterologously expressed Streptomyces type II polyketide synthase acyl carrier proteins, *FEBS Lett. 405*, 267−772.
33. Kay, L. E. (1995) Pulsed field gradient multi-dimensional NMR methods for the study of protein structure and dynamics in solution, *Prog. Biophys. Mol. Biol. 63*, 277−299.
34. Piotto, M., Saudek, V., and Sklenar, V. (1992) Gradient-tailored excitation for single-quantum NMR spectroscopy of aqueous solutions, *J. Biomol. NMR 2*, 661−665.
35. Delaglio, F., Grzesiek, S., Vuister, G. W., Zhu, G., Pfeifer, J., and Bax, A. (1995) NMRpipe: a multidimensional spectral processing system based on UNIX pipes, *J. Biomol. NMR 6*, 277−293.
36. Garrett, D. S., Powers, R., Gronenborn, A. M., and Clore, G. M. (1991) A common sense approach to peak picking in two-, three-, and four-dimensional spectra using automatic computer analysis of contour diagrams, *J. Magn. Reson. 95*, 214−220.
37. Wüthrich, K. (1986) *NMR of Proteins and Nucleic Acids*, John Wiley and Sons, New York.
38. Farrow, N. A., Muhandiram, R., Singer, A. U., Pascal, S. M., Kay, C. M., Gish, G., Shoelson, S. E., Pawson, T., Forman-Kay, J. D., and Kay, L. E. (1994) Backbone dynamics of a free and a phosphopeptide-complexed Src homology 2 domain studied by ^{15}N-relaxation, *Biochemistry 33*, 5984−6003.
39. Abragam, A. (1961) *Principles of Nuclear Magnetism*, Clarendon, Oxford.
40. Lipari, G., and Szabo, A. (1982a) A model-free approach to the interpretation of nuclear magnetic resonance relaxation in macromolecules I. Theory and range of validity, *J. Am. Chem. Soc. 104*, 4545−4549.
41. Lipari, G., and Szabo, A. (1982b) A model-free approach to the interpretation of nuclear magnetic resonance relaxation in macromolecules II. Theory and range of validity, *J. Am. Chem. Soc. 104*, 4549−4570.
42. Clore, G. M., Driscoll, P. C., Wingfield, P. T., and Gronenborn, A. M. (1990a) Analysis of the backbone dynamics of interleukin-1 beta using two-dimensional inverse detected heteronuclear ^{15}N-^{1}H NMR spectroscopy, *Biochemistry 29*, 7387−7401.
43. Clore, G. M., Szabo, A., Bax, A., Kay, L. E., Driscoll, P. C., and Gronenborn, A. M. (1990b) Deviations from the simple two-parameter model-free approach to the interpretation of nitrogen-15 nuclear magnetic relaxation of proteins, *J. Am. Chem. Soc. 112*, 4989−4991.
44. Lakowski, R. A., MacArthur, M. W., and Thornton, J. M. (1993) PROCHECK − a program to check the stereochemcial quality of protein structures, *J. Appl. Crystallogr. 26*, 283−291.
45. Koradi, R., Billeter, M., and Wuthrich, K. (1996) MOLMOL: a program for display and analysis of macromolecular structures, *J. Mol. Graphics 14*, 51−5, 29−32.
46. Henry, G. D., and Sykes, B. D. (1995) Determination of the rotational-dynamics and pH-dependence of the hydrogen-exchange rates of the arginine guanidine group using NMR spectroscopy, *J. Biomol. NMR 6*, 59−66.

47. Neuhaus, D., and Williamson, M. (1989) *The nuclear Overhauser effect in structural and conformational analysis*. VCH publishers Inc. New York.
48. Worsham, L. M. S., Earls, L., Jolly, C., Langston, K. G., M. Trent, S., and Ernst-Fonberg, M. L. (2003) Amino acid residues of *Escherichia coli* acyl carrier protein involved in heterologous protein interactions, *Biochemistry 42*, 167−176.
49. Gong, H., and Byers, D. M. (2003) Glutamate-41 of *Vibrio harveyi* acyl carrier protein is essential for fatty acid synthase but not acyl-ACP synthetase activity. *Biochem. Biophys. Res. Comm. 302*, 35−40.
50. Mulder, F. A. A., Hon, B., Muhandiram, D. R., Dahlquist, F. W., and Kay, L. E. (2000) Flexibility and ligand exchange in a buried cavity mutant of T4 lysozyme studied by multinuclear NMR, *Biochemistry 39*, 12614−12622.
51. Andrec, M., Hil, R. B., and Prestegard, J. H. (1995) Amide exchange rates in *Escherichia coli* and acyl carrier protein: Correlation with protein structure and dynamics, *Protein Sci. 4*, 983−993.

BI0342259